

NONLINEAR OPTICAL PHENOMENA

PACS numbers: 42.65. – k; 42.79.Dj; 72.40.+w
DOI: 10.1070/QE2008v038n08ABEH013712

Efficiency of optical poling of isotropic media

M.K. Balakirev, L.I. Vostrikova, V.A. Smirnov

***Abstract*. The spatial distributions of photoinduced electric fields are calculated based on the model of the current mechanism of optical poling of isotropic media and the efficiencies of the main poling schemes differing in the geometry of crossing beams are estimated. It is shown that the volume optical poling in a certain interval of small angles of crossing beams is the most promising for producing homogeneously distributed photoinduced electric structures of a large size.**

Keywords: *optical poling, three-wave interactions, isotropic media, coherent photogalvanic effect.*

1. Introduction

The optical poling (OP) is the formation of a long-lived spatially periodic electrostatic polarisation $\boldsymbol{P}(\boldsymbol{r})$ in a medium upon interaction of mutually coherent radiations with multiple frequencies [1]. It is known that in isotropic centrally symmetric media the OP leads to a reversible change in the symmetry by transforming the medium into optically uniaxial material in which nonlinear three-wave interactions become possible. Changes in the optical properties of the medium are present in many phenomena found experimentally, for example, photoinduced second harmonic generation (SHG) [2 – 4] and parametric light amplification [5] in gratings with the nonlinear susceptibility $\chi^{(2)}$, which appear due to the optical poling of the isotropic medium; Bragg self-diffraction and Raman light scattering from induced modulations Δn of the refractive index due to the OP [6, 7]; light-electric instability and stimulated increase in the anisotropy due to the OP, etc. [8, 9]. Processes of radiation conversion in media transformed during the OP attract attention of scientists both from the point of view of fundamental scientific research and due to the possibility of obtaining new broadband optoelectronic elements [10].

One of the microprocesses lying in the base of the OP medium is the appearance of the spatial asymmetry of optical transitions in it upon interaction of mutually coherent radiation with multiple frequencies. The asymmetry of transitions in the case of the OP upon the local [3] or spatial [due to coherent photogalvanic (CPG) current] [11, 12] separation of excited charge carriers leads to the increase in the spatially periodic electric field strength $\boldsymbol{E}(\boldsymbol{r})$ distributed inside the sample in time (in the region of interaction of poling radiations) and the medium polarisation $\boldsymbol{P}(\boldsymbol{r})$ corresponding to it. In weakly conducting media the appearing fields can achieve substantial quantities (no less than 10^6 V cm^{-1}) and remain for a long time by producing a stable quasi-stationary polarisation [9, 13].

The possibility of the OP of different isotropic media (glasses and waveguides [2, 4, 14, 15], polymer and hybrid organic and nonorganic films, etc. [10, 16, 17]) has been shown by now. The efficiency of the OP process, which is determined by the value of the field formed due to the OP and by its resultant distribution in the medium, is the key problem for applications. Two components contribute to the OP efficiency. The first one is related to the characteristic microscopic mechanisms of the spatial asymmetry of excitation in the medium. The second component is determined by the external OP conditions of the medium: parameters of the poling light, interaction geometry upon the OP, optical and electric properties of the medium. Under conditions of the predominant influence of the CPG current mechanism, the second component plays a significant role [12, 13]. The OP efficiency in this case depends not on the spatial asymmetry of local optical transitions but on the following redistribution of excited charge carriers, which leads to the formation of the resultant distribution of the induced OP field.

In this paper we studied theoretically the current mechanism of the optical poling of the isotropic medium. The spatial distributions of electric fields formed due to the OP are calculated within the framework of the phenomenological model of the appearance of the CPG effect in media. The OP efficiencies in the main geometries of the experiment are estimated and the possibility of realisation of different types of the optical poling is discussed.

2. Formulation of the problem

The current mechanism of the medium OP is based on the CPG effect [12, 13]. In the classical variant, the optical poling of the sample is performed by using high-power two-frequency mutually coherent radiation at the fundamental ($\boldsymbol{E}_1 = \boldsymbol{e}_1 E_1(\boldsymbol{r})\exp[\mathrm{i}(\boldsymbol{k}_1\boldsymbol{r} - \omega t + \psi_1)]$) and doubled ($\boldsymbol{E}_2 = \boldsymbol{e}_2 \times E_2(\boldsymbol{r})\exp[\mathrm{i}(\boldsymbol{k}_2\boldsymbol{r} - 2\omega t + \psi_2)]$) frequencies. It is assumed

M.K. Balakirev, L.I. Vostrikova, V.A. Smirnov Institute of Semiconductor Physics, Siberian Branch, Russian Academy of Sciences, prosp. Akad. Lavrent'eva 13, 630090 Novosibirsk, Russia;
e-mail: vostrik@isp.nsc.ru

Received 6 August 2007
Kvantovaya Elektronika **38** (8) 724 – 730 (2008)
Translated by I.A. Ulitkin

that due to this effect on the medium, a spatially modulated CPG current with the density $\boldsymbol{j}(\boldsymbol{r})$ and inverse vector $\Delta\boldsymbol{k} = 2\boldsymbol{k}_1 - \boldsymbol{k}_2$ appears inside the medium in the region of interaction of radiations:

$$\boldsymbol{j}(\boldsymbol{r}) = \boldsymbol{e}_j E_1^2(\boldsymbol{r}) E_2(\boldsymbol{r}) \cos(\Delta\boldsymbol{k}\boldsymbol{r} + \Delta\psi),$$
$$\boldsymbol{e}_j = \sigma_1 \boldsymbol{e}_1 (\boldsymbol{e}_1 \boldsymbol{e}_2) + \sigma_2 \boldsymbol{e}_2, \tag{1}$$

where σ_1 and σ_2 are the CPG constants; $\Delta\psi = 2\psi_1 - \psi_2$. The appearance of the light-induced current leads to the charge separation and formation of a spatially inhomogeneous distribution of the electric field $\boldsymbol{E}(\boldsymbol{r})$ inside the medium in time. The formation of the field in the medium is described by electrodynamic equations:

$$\frac{\partial \rho}{\partial t} + \operatorname{div}(\boldsymbol{j} + \boldsymbol{j}_c) = 0, \ \operatorname{div}(\varepsilon \boldsymbol{E}) = 4\pi\rho,$$

where ρ is the density of the induced charge in the OP region; $\boldsymbol{j}_c = \sigma \boldsymbol{E}$; σ and ε are the effective conductivity and permittivity of the medium, respectively. Under zero initial conditions the kinetics of the field increase due to the OP is described by the characteristic dependence $\boldsymbol{E}(t) \sim \tau[1 - \exp(-t/\tau)]$, where $\tau = \varepsilon/(4\pi\sigma)$ and its spatial distribution $\boldsymbol{E}(\boldsymbol{r}) = -\operatorname{grad}\phi(\boldsymbol{r})$ in the medium is determined by the Poisson equation for the potential $\phi(\boldsymbol{r})$:

$$\Delta\phi(\boldsymbol{r}) = \frac{1}{\sigma}\operatorname{div}\boldsymbol{j}, \ \Delta = \frac{\partial^2}{\partial x^2} + \frac{\partial^2}{\partial y^2} + \frac{\partial^2}{\partial z^2}. \tag{2}$$

The appearance of the field $\boldsymbol{E}$ causes a reverse change in the optical properties of the medium. Thus, the spatially modulated anisotropic addition to the refractive index $\Delta n \sim \chi^{(3)}\boldsymbol{E}^2$ [6] [$\chi^{(3)}$ is the third-order nonlinear susceptibility] and induced second-order polarisability $\chi^{(2)} \sim \chi^{(3)}\boldsymbol{E}$ [2] appear in the lowest orders of the field expansion of induced polarisation in the isotropic medium. It is obvious that the efficiency of the processes of linear and nonlinear light conversion observed in experiments on gratings Δn and $\chi^{(2)}$ directly depends on the OP efficiency of the medium determined by the quantity and distribution of the induced OP field.

In the following section of this paper we present the results of calculations of typical OP schemes used in experiments. The spatial distributions of the electric field induced due to the OP are theoretically analysed, the characteristics of different OP schemes are compared and their efficiencies are estimated.

3. Optical poling in the band geometry

Consider the simplest case. Let the light beams propagate due to the OP in the direction of the y axis, be unlimited along the x axis and have a Gaussian profile along the z axis:

$$E_1(\boldsymbol{r}) = E_{10}\exp\left(-\frac{z^2}{2w_1^2}\right), \quad E_2(\boldsymbol{r}) = E_{20}\exp\left(-\frac{z^2}{2w_2^2}\right), \tag{3}$$

where w_1 and w_2 are the radii of the beams of poling radiations at the half-maximum intensity level in the focal plane. This situation appears in the experiment upon focusing collimated beams by a cylindrical lens. The OP region has the form of a thin extended band.

For the CPG current density $\boldsymbol{j}$, we obtain the expression in the band OP geometry:

$$\boldsymbol{j}(\boldsymbol{r}) = \boldsymbol{e}_j E_{10}^2 E_{20}\exp\left(-\frac{z^2}{2w^2}\right)\cos(\Delta k y), \tag{4}$$

where

$$w^2 = \frac{w_1^2 w_2^2}{2w_2^2 + w_1^2};$$

$e_{jz} = \sigma_1 \cos\alpha_1 \cos\varphi_0 + \sigma_2 \cos\alpha_2$, $e_{jx} = \sigma_1 \sin\alpha_1 \cos\varphi_0 + \sigma_2 \times \sin\alpha_2$ are the nonzero components; φ_0 is the angle between the vectors $\boldsymbol{e}_1$ and $\boldsymbol{e}_2$; α_1 and α_2 are the angles between the vectors $\boldsymbol{e}_1$ and $\boldsymbol{e}_2$ and the z axis, respectively.

For convenience of the solution, we introduced the notations $\eta = \Delta k w$, $E_0 = E_{10}^2 E_{20}$ and pass to dimensionless variables:

$$i \to \frac{i}{w} \ (i = x, y, z), \ \ \boldsymbol{j}(\boldsymbol{r}) \to \frac{\boldsymbol{j}(\boldsymbol{r})}{E_0},$$
$$\boldsymbol{j}(\boldsymbol{r}) = \boldsymbol{e}_j \exp\left(-\frac{z^2}{2}\right)\cos(\eta y), \ \phi(\boldsymbol{r}) \to \phi(\boldsymbol{r})\frac{\sigma}{E_0}. \tag{5}$$

Taking into account the periodicity of the grating of the current density $\boldsymbol{j}(\boldsymbol{r})$, the solution for the potential is sought for in the form $\phi(\boldsymbol{r}) = \phi(y, z) = \phi(z)\cos(\eta y)$ with the boundary conditions $\phi(z \to \pm\infty) = 0$. The function $\phi(z)$ is found from the solution of the equation

$$\left(\frac{\partial^2}{\partial z^2} - \eta^2\right)\phi(z) = -\boldsymbol{e}_{jz} z \exp\left(-\frac{z^2}{2}\right) \tag{6}$$

and has the form

$$\phi(z) = \boldsymbol{e}_{jz}\sqrt{\frac{\pi}{8}}\exp\left(\frac{\eta^2}{2}\right)\left[\exp(-\eta z)\operatorname{erf}\left(\frac{\eta - z}{\sqrt{2}}\right)\right.$$
$$\left. - \exp(\eta z)\operatorname{erf}\left(\frac{\eta + z}{\sqrt{2}}\right)\right]. \tag{7}$$

The function $\operatorname{erf}(\xi)$ is determined by the expression

$$\operatorname{erf}(\xi) = \frac{2}{\sqrt{\pi}}\int_{\xi}^{+\infty}\exp(-\xi^2)\mathrm{d}\xi. \tag{8}$$

The final expressions for the distribution of field components in the medium, which correspond to the potential $\phi(y, z)$, have the form in the model of the OP band geometry

$$E_y(y, z) = \phi(z)\eta\sin(\eta y),$$
$$E_z(y, z) = -\frac{\partial}{\partial z}[\phi(z)]\cos(\eta y) \tag{9}$$
$$= e_{jz}\left\{\sqrt{\frac{\pi}{8}}\eta\exp\left(\frac{\eta^2}{2}\right)\left[\exp(-\eta z)\operatorname{erf}\left(\frac{\eta - z}{\sqrt{2}}\right) + \right.\right.$$

$$+ \exp(\eta z)\mathrm{erf}\left(\frac{\eta + z}{\sqrt{2}}\right)\Bigg] - \exp\left(-\frac{z^2}{2}\right)\Bigg\}\cos(\eta y).$$

Before analysing the obtained expressions, note the following. For the typical experimental values $w = 1 - 100$ μm, which reflect the effective width of the OP region [see expression (4)], and the modulus of the inverse vector $\Delta k = 0.1 - 50$ μm^{-1} of induced gratings, we have $\eta = 0.1 - 5 \times 10^3$. Gratings of a small size with a low number of periods correspond to low η and gratings of the largest size with the maximum number of periods correspond to large η. It is obvious that induced gratings obtained at relatively large values of η are more high-contrast ones. The mentioned fact will be taken into account in the following analysis.

Figure 1 shows the distributions of the field components E_y and E_z along the z axis derived from expressions (9) for $\eta = 0.1$, 1, 5 and 10, which correspond in the experiment to the field-induced gratings with the transverse size up to ~ 100 μm. One can see that the component E_z (in the direction perpendicular to the propagation direction of the poling radiation) is maximal in the centre of the OP region for $z = 0$ and rapidly decreases with moving away from the centre. The component E_y (in the direction parallel to the propagation direction of the poling radiation) is, on the contrary, equal to zero in the centre of the OP region and increases with moving away from the centre. For $\eta \to 0$, the component $E_y \to 0$, while $E_z \to 1$. Therefore, the region of low values η is the most optimal for the field component E_z, while for the component E_y it is the region $\eta \sim 1$.

The field components E_y and E_z decrease with increasing η and tend to zero for $\eta \to \infty$. Taking into account the asymptotics of the function $\mathrm{erf}(\xi)$ at large values of its argument, we have $E_y \sim \eta^{-1}$, $E_z \sim \eta^{-2}$. One can see that the induced field quickly decreases with increasing η; however, the component E_y decreases significantly slower than E_z. The main disadvantage of the OP band geometry is the impossibility of producing contrast gratings with η large enough. When η substantially increases, the OP region broadens and the charges induced by poling begin to accumulate along the boundary of this region. As a result, the field is concentrated near the boundary and quite rapidly (proportionally to $1/\Delta k$) decreases inside the OP region (Fig. 1, the curve for $\eta = 10$). In this case, the OP efficiency drastically decreases. It obvious that the decrease in the OP efficiency with increasing η has an effect on linear and nonlinear optical conversions taking place in the gratings Δn and $\chi^{(2)}$ induced in the medium. For example, when the component E_z is used in the experiment the intensity $I_g \sim (\chi^{(2)})^2 \sim (\chi^{(3)} E_z)^2$ of the three-wave interaction will decrease proportionally to η^{-4}.

Note, however, that the OP band geometry can be efficient due to a large length of the field-induced gratings. Thus, by illuminating the grating with light propagating in the plane xy, it is possible to obtain the Bragg diffraction and harmonic generation at the maximum interaction length. The band scheme also has a wide spectral range of the radiation conversion. When the incidence angle of radiation with the specified frequency Ω is selected in the xy plane so that the condition $2\boldsymbol{k}_\Omega - \boldsymbol{k}_{2\Omega} = \Delta\boldsymbol{k}$ is fulfilled [thus compensating for the phase detuning for the harmonic generation with the frequency 2Ω due to the in-phase variations in $\chi^{(2)} \sim \chi^{(3)} E$], the required angle of incidence turns low due to the smallness of the ratio $\Delta k/k_\Omega$ and the region of the efficient frequency conversion is rather broad if the visible and near-IR radiation is used.

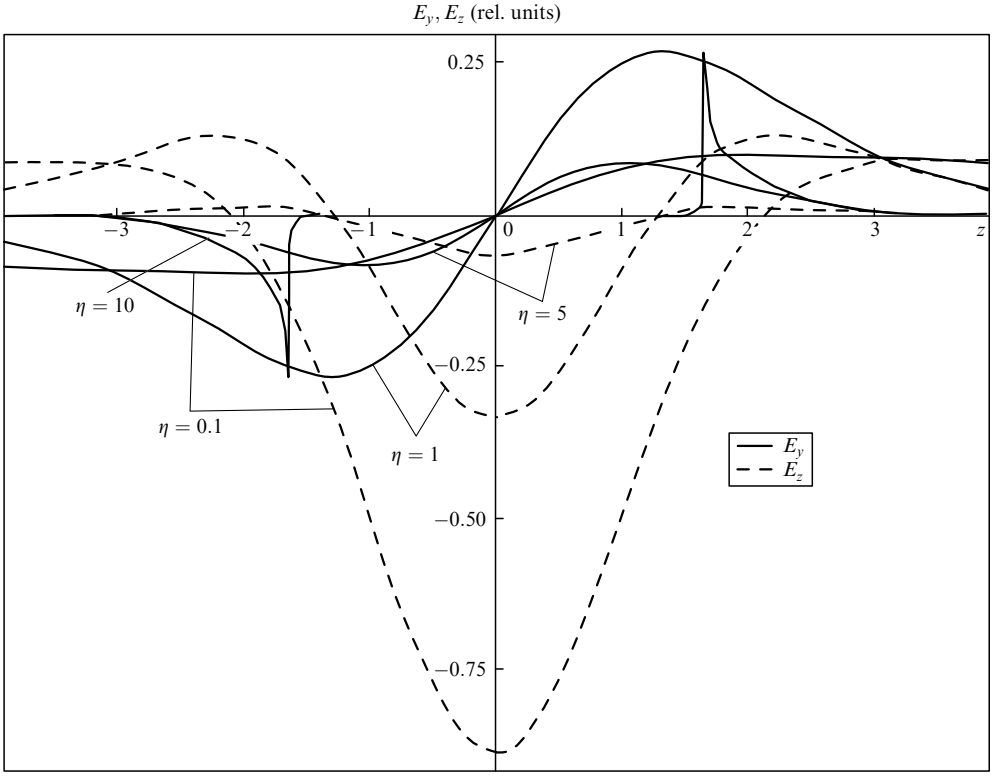

Figure 1. Distribution of the electric field components in the medium induced by the OP in the band geometry.

4. Optical poling in the cylindrical geometry

Let the coaxial radiation beams at the fundamental and doubled frequencies propagate due to the OP along the y axis and focus in the extended region with waist centre for $y = 0$. We assume that the radiation is polarised along the z axis and the beam divergence is neglected. This type of the OP is typical of the waveguide and fibre materials and, for example, was studied experimentally in photoinduced SHG in glass waveguides [2, 3] and in bulky samples [4, 10, 14]. The OP region in this case has the form of a cylinder.

The expression for the CPG current density in dimensionless variables (5) for the selected OP cylindrical geometry has the form

$$\boldsymbol{j}(\boldsymbol{r}) = \boldsymbol{e}_{jz} \exp\left(-\frac{\boldsymbol{r}_\perp^2}{2}\right) \cos(\eta y), \quad \boldsymbol{r}_\perp^2 = x^2 + z^2. \tag{10}$$

By using expression (2) and taking the periodicity $\boldsymbol{j}(\boldsymbol{r})$ into account, we will write the equation for the induced field components $\boldsymbol{E}(\boldsymbol{r})$:

$$\left(\frac{\partial^2}{\partial x^2} + \frac{\partial^2}{\partial z^2} - \eta^2\right) E_x(x,z) = -e_{jz} xz \exp\left(-\frac{\boldsymbol{r}_\perp^2}{2}\right),$$

$$\left(\frac{\partial^2}{\partial x^2} + \frac{\partial^2}{\partial z^2} - \eta^2\right) E_y(x,z) = -e_{jz} \eta z \exp\left(-\frac{\boldsymbol{r}_\perp^2}{2}\right), \tag{11}$$

$$\left(\frac{\partial^2}{\partial x^2} + \frac{\partial^2}{\partial z^2} - \eta^2\right) E_z(x,z) = e_{jz}(1 - z^2) \exp\left(-\frac{\boldsymbol{r}_\perp^2}{2}\right),$$

where

$$E_{x,z}(x,y,z) = E_{x,z}(x,z)\cos(\eta y); E_y(x,y,z) = E_y(x,z)\sin(\eta y).$$

To solve expression (11), we use first the Fourier transform over x and z and then pass to the cylindrical variables in the integrals. In this case, $k_x = k\sin(\theta + \varphi)$, $k_z = k\cos(\theta + \varphi)$, where θ is the angle between the vectors $\boldsymbol{r}_\perp$ and $\boldsymbol{k}$ and φ is the angle between the vector $\boldsymbol{r}_\perp$ and the axis z. As a result, after integrating over θ, the expression for the field components can be derived in the integral form:

$$E_x(r_\perp, \varphi) = -2e_{jz}\sin(2\varphi)\int_0^\infty \frac{k^3 \exp(-k^2/2) J_2(kr_\perp)}{k^2 + \eta^2}\,\mathrm{d}k;$$

$$E_y(r_\perp, \varphi) = -e_{jz}\eta\cos\varphi\int_0^\infty \frac{\mathrm{i}k^2 \exp(-k^2/2) J_1(kr_\perp)}{k^2 + \eta^2}\,\mathrm{d}k; \tag{12}$$

$$E_z(r_\perp, \varphi) = e_{jz} \times \int_0^\infty \frac{k^3 \exp(-k^2/2)[J_0(kr_\perp) - 2\cos(2\varphi) J_2(kr_\perp)]}{k^2 + \eta^2}\,\mathrm{d}k.$$

Here, $J_m(kr_\perp)$ is the Bessel function of the corresponding mth order ($m = 0, 1, 2$).

Solutions of system (12) in the analytic form are absent and it is possible to study them by using only numerical methods. However, it follows from (12) that similar to the OP band geometry, in the case of the cylindrical geometry the field component E_y is also zero in the centre of the OP region, while the component E_z coinciding with the direction of the CPG current is maximal. The dependence of E_z on η in the central OP region (on the beam axis) is described by the integral exponential:

$$E_z(r_\perp = 0) = e_{jz}\left[1 + \frac{\eta^2}{2}\exp\left(\frac{\eta^2}{2}\right)\mathrm{Ei}\left(-\frac{\eta^2}{2}\right)\right],$$
$$\mathrm{Ei}(\xi) = \int_{-\infty}^{\xi} \frac{\mathrm{e}^\xi}{\xi}\,\mathrm{d}\xi. \tag{13}$$

By using the asymptotics of the $\mathrm{Ei}(-\eta^2/2)$ function for large arguments, we obtain the characteristic dependence $E_z \sim \eta^{-2}$. One can see that the poling efficiency also sharply decreases with increasing η in the OP cylindrical geometry, which prevents the formation of contrast gratings of a large size. This fact is confirmed in experiments. For example, in the known research of the photoinduced SHG in waveguides, the radiation conversion efficiency already tends to zero, when the diameter of the OP region exceeds 20 μm [2]. The recently performed studies of the three-wave interaction in induced gratings $\chi^{(2)}$ in different glass samples by using the OP cylindrical geometry and preserving the constant power density of poling radiations in the OP region also show a characteristic decrease in the efficiency with increasing the OP region.

5. Volume poling

Consider the most general case of the medium OP by crossing Gaussian beams. This type of the OP was used by us in recent experiments on observation of the diffraction of light from volume Bragg refractive index gratings photoinduced due to poling [6, 7] and parametric light amplification [5] and photoinduced SHG [4] on gratings $\chi^{(2)}$ produced upon optical poling in the volume medium.

We will show that compared to the above types of the OP, the volume poling has an important advantage associated with the possibility of changing the properties of the grating produced in the medium.

We will write expressions for the period $\Lambda = 2\pi/\Delta k$ of the grating of the CPG current density $\boldsymbol{j}(\boldsymbol{r})$, which is photoinduced due to the volume OP, and for the angle $\beta = (\widehat{\boldsymbol{k}_1, \Delta\boldsymbol{k}})$ of its orientation with respect to the direction of the fundamental radiation, which is used upon optical poling:

$$\Lambda = h\frac{\lambda_1}{2n_2}, \ \beta = \arcsin(h\sin\alpha),$$
$$h = \left[1 + \left(\frac{n_1}{n_2}\right)^2 - 2\frac{n_1}{n_2}\cos\alpha\right]^{-1/2}. \tag{14}$$

Here, λ_1 is the radiation wavelength at the fundamental frequency; $n_{1,2}$ are the refractive indices of the medium for radiation at the fundamental and doubled frequencies, respectively; α is the angle of beam divergence upon OP inside the sample (the poling angle). Figure 2 shows the dependences $\Lambda(\alpha)$ and $\beta(\alpha)$ for $\lambda_1 = 1.06$ μm, $\delta n = n_2 - n_1 = 5 \times 10^{-2}$, $n_1/n_2 = 0.97$ and $n_{1,2} \approx 1.5$, which are typical for experiments on the OP in glass media.

One can see from Fig. 2 that the distinct feature of the volume OP in the region of small poling angles is a fast change in the dependences $\Lambda(\alpha)$ and $\beta(\alpha)$ with increasing α. By changing the poling angle α, the period Λ of the grating of the current density $\boldsymbol{j}(\boldsymbol{r})$ appearing in the medium varies in

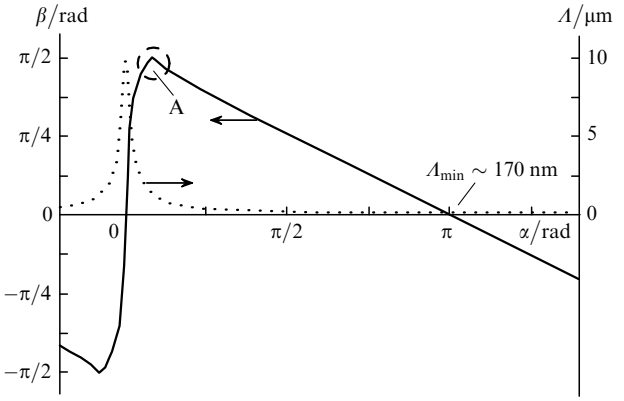

Figure 2. Dependences of the period Λ and orientation angle β of the grating of the CPG current upon the volume OP on the divergence angle α of the radiation beams.

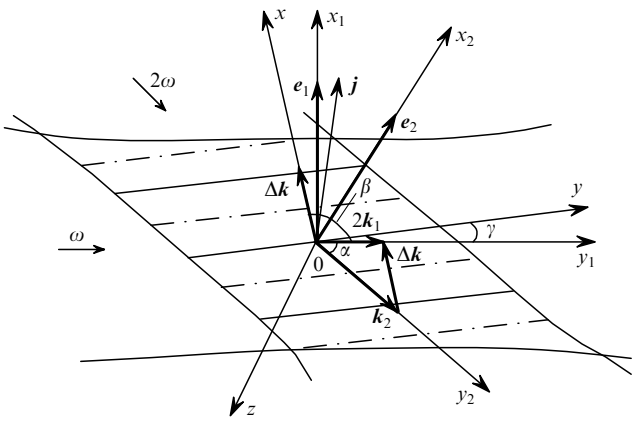

Figure 3. Formation of the field grating upon the volume OP.

a broad range (almost by two orders of magnitude): from $\Lambda_{\max} = \lambda_1/(2\delta n) \sim 10^4$ nm to $\Lambda_{\min} \approx \lambda_1/(4n_1) \sim 170$ nm (tenth fractions of the light wavelength). One can also see from Fig. 2 that the grating orientation in the medium strongly depends on the poling angle. Indeed, when α varies within several degrees near the zero, the angle β takes values from $-\pi/2$ до $\pi/2$. This means that upon the volume OP it is possible to produce in the medium a grating with almost any (from parallel to perpendicular) orientation of its planes with respect to the direction $\boldsymbol{j}(\boldsymbol{r})$*.

The most interesting in Fig. 2 is the marked region A of small poling angles in which the condition $\beta \approx \pi/2$ is fulfilled and the vectors $\boldsymbol{j}(\boldsymbol{r})$ and $\Delta\boldsymbol{k}$ are virtually parallel to each other. The charge carriers in this case are separated mainly in the direction perpendicular to the planes of the grating being produced in the medium, the separation being accompanied by the accumulation of the effect near these planes. It is obvious that this charge separation should favour the formation of the volume periodic field structure homogeneously distributed in the entire OP region. Note that in the OP types considered above (in band and cylindrical geometries) this possibility was absent because the condition $\boldsymbol{j}(\boldsymbol{r}) \perp \Delta\boldsymbol{k}$ was always fulfilled and only the longitudinal CPG current, directed along the grating planes, existed. In calculations below we will pay attention to the case $\boldsymbol{j}(\boldsymbol{r}) \| \Delta\boldsymbol{k}$ in the region of small poling angles.

Consider the formation of the field in the medium upon volume optical poling. We assume that the sample OP is performed by two Gaussian beams of mutually coherent radiations at the fundamental (ω) and doubled (2ω) frequencies, the beams being focused inside the medium and intersecting at a small poling angle α (Fig. 3). We select the origin of coordinates in the point of intersection of the beam axes, which coincides with the centres of their waists. We assume that the poling radiations with the wave vectors $\boldsymbol{k}_1$ and $\boldsymbol{k}_2$ propagate along the axes y_1 and y_2, respectively. In this case, the inverse vector formed in the medium of the grating of the CPG current $\Delta\boldsymbol{k} = 2\boldsymbol{k}_1 - \boldsymbol{k}_2$ will be located in the plane y_1y_2 (Fig. 3). We consider that the poling radiations are linearly polarised and their polarisation vectors $\boldsymbol{e}_1$ and $\boldsymbol{e}_2$ are directed along the axes x_1 and x_2, respectively. One can see from Fig. 3 that the case $\boldsymbol{j}(\boldsymbol{r}) \| \Delta\boldsymbol{k}$ typical of the volume OP, in which the CPG current will be mainly directed perpendicular to the planes of the grating being formed in the medium, appears under the condition that the polarisation vectors $\boldsymbol{e}_1$ and $\boldsymbol{e}_2$ of poling radiations lie in the plane y_1y_2.

We select for calculations the coordinates system xy related with the grating of the current: the x axis is directed along the grating vector $\Delta\boldsymbol{k}$, while the y axis – along the grating planes. We denote the angle between the axes y_1 and y by $\gamma = \beta - 90^\circ$ (Fig. 3). In this case, the expression for the CPG current density in the coordinate system of the grating in dimensionless variables (5) will be written in the form

$$\boldsymbol{j}(\boldsymbol{r}) = \boldsymbol{e}_j \exp\left[-\frac{1}{2}(ax^2 + by^2 + cxy + z^2)\right]\cos(\eta x), \quad (15)$$

where

$$a = 1 - b;\ b = \frac{2w^2}{w_1^2}\sin^2\gamma + \frac{w^2}{w_2^2}\sin^2(\gamma + \alpha);$$
$$c = \frac{2w^2}{w_1^2}\sin 2\gamma + \frac{w^2}{w_2^2}\sin 2(\gamma + \alpha). \quad (16)$$

Upon the volume OP, the components $e_{jx} = \sigma_1 \cos\gamma \cos\alpha + \sigma_2 \cos(\alpha + \gamma)$ and $e_{jy} = \sigma_1 \sin\gamma \cos\alpha + \sigma_2 \sin(\alpha + \gamma)$ are nonzero for the characteristic case $\boldsymbol{j}(\boldsymbol{r}) \| \Delta\boldsymbol{k}$. In the range of small angles α and γ under study, a number of conditions necessary for calculations is fulfilled:

$$a, b, c > 0,\ b \ll c \ll a \lesssim 1,\ s = \frac{e_{jy}}{e_{jx}} \approx \gamma + \frac{\alpha\sigma_2}{(\sigma_1 + \sigma_2)} \ll 1. \quad (17)$$

Note also that at small poling angles α, the parameter η, nevertheless, should be large enough, so that at least several grating periods fitted the waist diameter in the OP region (otherwise, it is unreasonable to speak about the presence of the grating).

When the dimensionless variables are used in the coordinate system of the grating, the expression for the potential distribution $\phi(\boldsymbol{r})$ in the medium for the case of the volume OP under study is written in the form

$$\Delta\phi(\boldsymbol{r}) = e_{jx} I(z)\left(\frac{\partial}{\partial x} + s\frac{\partial}{\partial y}\right)[I(x, y)\cos(\eta x)],$$

*Note that the direction $\boldsymbol{j}(\boldsymbol{r})$ in the medium is determined by the polarisation of poling radiations [see expression (1)] and is virtually perpendicular to the direction of light propagation at small poling angles.

$$I(z) = \exp\left(-\frac{z^2}{2}\right), \tag{18}$$

$$I(x,y) = \exp\left[-\frac{1}{2}(ax^2 + by^2 + cxy)\right].$$

We seek for the solution of Eqn (18) with the help of the three-dimensional Fourier transform successively over coordinates z, y and x taking (17) into account. Upon inverse transform in the case of integration over the complex variables, we take into account that the small vicinities of the points $k_x = 0, \pm\eta$ make the main contribution.

As a result, for the potential distribution $\phi(\mathbf{r})$ in the volume of the medium we obtain the expression

$$\begin{aligned}
&\phi(\mathbf{r}) = e_{jx}\phi(z,\eta)I(x,y)[(gx+py)\cos(\eta x) - \eta\sin(\eta x)],\\
&\phi(z,\eta) = \sqrt{\frac{\pi}{2}}\frac{1}{\eta}\exp\left(\frac{\eta^2}{2} - \eta|z|\right)\\
&\quad\times\left[\mathrm{erf}\left(\frac{\eta - z}{\sqrt{2}}\right) - \mathrm{erf}\left(\frac{\eta + z}{\sqrt{2}}\right)\right],\\
&g = a + \frac{cs}{2},\ p = \frac{c}{2} + bs.
\end{aligned} \tag{19}$$

Expressions for the distribution of the field components in the medium corresponding to this potential have the form

$$\begin{aligned}
E_x &= e_{jx}\phi(z,\eta)I(x,y)\sin(\eta x + \psi_x)\\
&\times\left\{\left[agx^2 + \left(ap + \frac{c}{2}g\right)xy + \frac{c}{2}py^2 + \eta^2 - g\right]^2\right.\\
&\quad\left.+\eta^2 s^2\left(by + \frac{c}{2}x\right)^2\right\}^{1/2},\\
E_y &= e_{jx}\phi(z,\eta)I(x,y)\cos(\eta x + \psi_y)\\
&\times\left\{\left[\frac{c}{2}gx^2 + \left(\frac{c}{2}p + bg\right)xy + bpy^2 - p\right]^2\right.\\
&\quad\left.+\eta^2\left(by + \frac{c}{2}x\right)^2\right\}^{1/2},\\
E_z &= e_{jx}I(x,y)[(gx+py)^2 + \eta^2]^{1/2}\cos(\eta x + \psi_z)\\
&\quad\times\left[\eta\phi(z,\eta)\Theta(z) - \frac{2}{\eta}\exp\left(-\frac{z^2}{2} - \eta|z|\right)\cosh(\eta z)\right],
\end{aligned} \tag{20}$$

where $\Theta(z)$ is the theta-function;

$$\begin{aligned}
\psi_x &= \arctan\left[\frac{agx^2 + (ap + cg/2)xy + cpy^2/2 + \eta^2 - g}{\eta s(by + cx/2)}\right];\\
\psi_y &= \arctan\left[\frac{\eta(by + cx/2)}{cgx^2/2 + (cp/2 + bg)xy + bpy^2 - p}\right];\\
\psi_z &= \arctan\left(\frac{\eta}{gx + py}\right).
\end{aligned} \tag{21}$$

Analysis of expressions (20) for $\eta \gg 1$ shows that similarly to the OP in the band and cylindrical geometries considered above, the field components E_y and E_z in the case of the volume OP also rapidly decrease with increasing η (proportionally to η^{-1}). However, the behaviour of the component E_x in the volume OP differs from its behaviour upon the optical poling in the above-mentioned geometries. It follows from the analysis of expressions for E_x in (20) for $\eta \gg 1$ at different points of the OP region that an increase in η with increasing the OP region does not lead to a significant decrease in the field component E_x. Note that expressions (20) were obtained for dimensionless variables and field components normalised to the maximum value $E_0 = E_{10}^2 E_{20}$, which characterises the influence on the OP intensities of interacting waves. In this case, changes in the calculated field components according to (20) directly affect changes in the field distribution in the OP region. Therefore, the volume poling with the formation of the field component E_x is optimal for creating large photoinduced field structures homogeneously distributed in the OP region.

6. Experiment

To confirm the possibility of obtaining large field structures with the help of the volume OP, we performed experiments to study the Bragg diffraction and nonlinear transformation of waves from the modulations Δn and $\chi^{(2)}$ formed due to the volume OP. From the set of industrial glasses, we selected oxide K8 glass, which exhibited the highest OP efficiency. The volume optical poling of the sample was performed for the poling angle $\alpha \sim 3^\circ - 4^\circ$ from the region A in Fig. 2. Mutually coherent radiation beams at the fundamental and doubled frequencies from a pulsed 1.079-μm $Nd^{3+}:YAlO_3$ laser were focused in the region of size ~ 250 μm and intersected at the angle α inside the sample. Radiation polarisations were selected in accordance with the above discussed condition of the volume OP. The maximum pulse energy of the primary radiation was ~ 18 mJ, the pulse duration was approximately 15 ns and the pulse repetition rate was 12.5 Hz. The peak radiation intensities at the fundamental and doubled frequencies in the focus were $\sim 10^9$ and $\sim 10^8$ W cm^{-2}, respectively. Radiations appearing due to the Bragg diffraction and SHG on gratings Δn and $\chi^{(2)}$ written by the volume OP upon their irradiation at the fundamental frequency were recorded in the far-field region by using a photoelectronic multiplier. The used equipment allowed real-time recording and processing of the pulse power of the diffracted radiation and radiation at the second harmonic frequency by using a PC. The threshold sensitivity of the recording system was 1 mW pulse^{-1}. The gratings Δn and $\chi^{(2)}$ written in the glass by using the OP were stable and remained for several hours in the absence of the external action. The process of writing gratings was fully reversible and was not accompanied by the structural changes in the samples. The writing kinetics and relaxation of gratings as well as the results of observations of radiations induced due to SHG and Bragg diffraction are presented in [4, 5].

To diagnose the distribution homogeneity of induced gratings during the observation of signals appearing due to Bragg diffraction and SHG, the OP region was scanned with a narrow beam from a 0.6327-μm He–Ne laser along the length and width of the gratings [along the axes y_1 and x_1, respectively (Fig. 3)]. The radiation from the He–Ne laser

partially 'erased' the grating of the field in the illuminated region. As a result, dips were observed in signals appearing upon diffraction and SHG. The scanning radiation intensity was ~ 30 W cm^{-2}. The irradiation time was ~ 2 min with the interval of 10 min between irradiations, the diameters of the beams from the He – Ne laser were ~ 200 and ~ 20 μm upon scanning along the length and width of the grating, respectively.

Figure 4 shows the dependences of the diffracted radiation intensity upon scanning by the He – Ne-laser radiation the region of the field grating in the medium produced by the volume OP. One can see that the experimentally obtained grating width is ~ 180 μm and its length is ~ 7 mm. The inset in Fig. 4 presents the spatial intensity distribution of the diffracted radiation in the plane x_1y_1 in the direction perpendicular to the propagation direction of the diffracted wave, which demonstrates that the diffraction proceeds in the entire region of the grating and the intensity distribution has a characteristic Gaussian profile. Such dependences were also obtained by studying a signal appearing on the grating $\chi^{(2)}$ upon SHG due to the volume OP. Note, finally, that when the polarisations of the poling radiations were rotated by 90°, the observed signals appearing upon diffraction and SHG were $\sim 10^4 - 10^5$ times weaker and were detected by scanning He – Ne-laser radiation only near the boundary of the OP region. This indicates that a homogeneous volume field grating is not formed in the medium. The results obtained in the experiment agree with the calculated data.

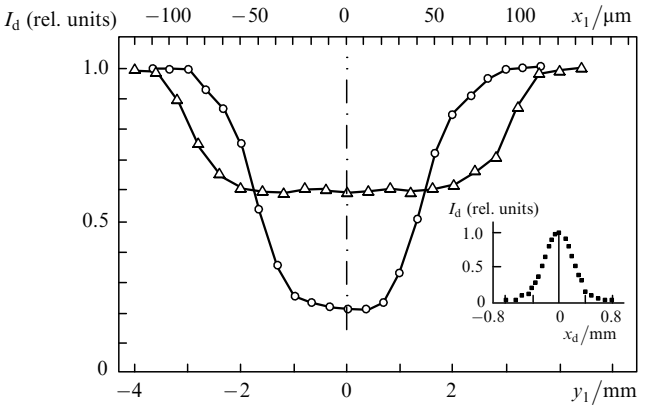

Figure 4. Dependences of the intensity I_d of radiation diffracted in the Bragg geometry upon scanning the region of the field grating by the He – Ne-laser radiation along the length (△) and width (○) of the grating. The inset shows the intensity distribution of the diffracted light (x_d is the displacement from the beam axis along the direction lying in the plane x_1y_1 and perpendicular to the diffraction direction).

7. Conclusions

An analysis of the efficiencies of typical experimental OP schemes has been performed in this paper by using the model of the current mechanism of the OP of isotropic media. It has been shown that the quantity and distribution of the field induced in the medium substantially depend on the interaction geometry during the OP. Spatial distributions of the electric fields have been studied. It has been shown theoretically and experimentally verified that under certain condition it is possible to produce large induced field structures distributed in the volume of the medium by using the volume OP. The results have been obtained, which can be hereafter used to study the OP of different media and to develop optoelectronic devices.

Acknowledgements. This work was supported by the Russian Foundation for Basic Research (Grant Nos 05-02-17220 and 06-08-01502).

References

1. Antonyuk B.P. *Opt. Commun.*, **174**, 427 (2000).
2. Dianov E.M., Starodubov D.S. *Kvantovaya Elektron.*, **22**, 419 (1995) [*Quantum Electron.*, **25**, 395 (1995)].
3. Antonyuk B.P., Antonyuk V.B. *Usp. Fiz. Nauk*, **171**, 61 (2001).
4. Balakirev M.K., Vostrikova L.I., Smirnov V.A., Kityk I.V., Ebothe J. *Phys. Rev. A*, **67**, 023806 (2003).
5. Balakirev M.K., Smirnov V.A., Vostrikova L.I. *Opt. Commun.*, **178**, 181 (2000).
6. Balakirev M.K., Vostrikova L.I., Smirnov V.A. *Kvantovaya Elektron.*, **32**, 416 (2002) [*Quantum Electron.*, **32**, 416 (2002)].
7. Balakirev M.K., Smirnov V.A., Vostrikova L.I. *J. Opt. A: Pure Appl. Opt.*, **5**, 437 (2003).
8. Balakirev M.K., Vostrikova L.I., Smirnov V.A., Entin M.V. *Pis'ma Zh. Eksp. Teor. Fiz.*, **80**, 32 (2004).
9. Antonyuk B.P. *Light Driven Self-Organization* (New-York: Nova Science, 2003).
10. Hirao K., Qian G., Wang M., et al. *Chem. Phys. Lett.*, **381**, 677 (2003).
11. Baskin E.M., Entin M.V. *Pis'ma Zh. Eksp. Teor. Fiz.*, **48**, 554 (1988).
12. Sulimov V.B. *Zh. Eksper. Teor. Fiz.*, **101**, 1749 (1992).
13. Baskin E.M., Entin M.V. *Coherent Control in Atoms, Molecules, and Semiconductors* (Dordrecht & Boston: Kluwer Acad. Publ., 1999).
14. Shchavelev O.S., Shchavelev K.O., Kundikova G.T., Churikov V.M., et al. *Opt. Zh.*, **68**, 49 (2001).
15. Tsutsumi N., Nakatani K. *Opt. Commun.*, **259**, 852 (2006).
16. Jia Y., Wang G., Guo B., Su W., Zhang Q. *J. Opt. A: Pure Appl. Opt.*, **6**, 833 (2004).
17. Odane C., Tsutsumi N. *J. Opt. Soc. Am. B,* **20**, 1514 (2003).